PERGAMON

International Journal of Heat and Mass Transfer 42 (1999) 2171–2185

International Journal of HEAT and MASS TRANSFER

Energy wheel effectiveness: part II—correlations

C.J. Simonson, R.W. Besant*

Department of Mechanical Engineering, University of Saskatchewan, 57 Campus Drive, Saskatoon, SK, Canada S7N 5A9

Received 21 April 1998; in final form 17 September 1998

Abstract

Effectiveness correlations are presented which allow the designer to predict the sensible, latent and total effectiveness of energy wheels when the operating conditions are known. The correlations agree with simulation data within $\pm 2.5\%$ for sensible, latent and total effectiveness when the desiccant coating on the energy wheel has a linear sorption curve. The sensitivity of the sorption curve and operating condition factor are studied and the use of the design correlations is shown with an example.

Nomenclature

A_s heat and mass transfer surface area on the supply or exhaust side [m^2]
A_m total cross-sectional area of the matrix [m^2]
a^* height to base ratio of a sine duct
C constant describing the shape of the sorption curve
C_λ axial conduction correction factor
C^* ratio of the minimum to maximum heat capacity rate of the air streams
Cr_o^* overall matrix heat (or moisture) capacity ratio
Crm_o^* overall matrix moisture capacity ratio
C_p specific heat [J kg^{-1} K^{-1}]
D diameter of the energy wheel [m]
D_h hydraulic diameter of one tube in the energy wheel [m]
H^* operating condition factor that represents the ratio of latent to sensible enthalpy differences between the inlets of the energy wheel
h convective heat transfer coefficient [W m^{-2} K^{-1}]
k thermal conductivity [W m^{-1} K^{-1}]
L length of the heat exchanger [m]
M total mass [kg]
$\dot{m}$ mass flow rate of dry air [kg s^{-1}]
N angular speed of the wheel [cycles s^{-1}]
Nu Nusselt number
NTU_o overall number of transfer units
T bulk temperature [K or °C]
u mass fraction of water in the desiccant [kg_w kg_d^{-1}]
Wm empirical coefficient used in the sorption isotherm describing the maximum moisture capacity of the desiccant [kg_w kg_d^{-1}].

Greek symbols
β surface area density [m^2 m^3]
Δ difference between supply inlet and exhaust inlet conditions or change in sensible effectiveness due to moisture transfer
ε effectiveness
ε_s sensible heat transfer effectiveness
ε_l latent heat transfer (or moisture transfer) effectiveness
ε_t total enthalpy effectiveness
η fraction of the phase change energy that is delivered directly to the air
λ dimensionless axial conduction
ρ density [kg m^{-3}]
σ volume fraction
Φ parameter used in the axial conduction correction
ϕ relative humidity
χ general dependent variable.

Subscripts
a air
ave average between the supply and exhaust inlet conditions
e exhaust side
d desiccant
dry dry properties
ht dimensionless heat transfer group for energy wheels
i inlet

* Corresponding author. Fax: 001 306 966 5427

0017–9310/99/$ - see front matter
PII: S0017–9310(98)00327–5

m matrix (including support material, desiccant and moisture)
min minimum
mt dimensionless moisture transfer group for energy wheels
o outlet or overall dimensionless group applying to the entire wheel
s supply side
sup support material.

1. Introduction

Designing heat exchangers and predicting their performance is often done using the ε–NTU method, which is well established for sensible heat exchangers [1, 2]. The classical definition of effectiveness (ε), as defined in many heat transfer and heat exchanger books [1–3], applies to sensible energy transfer with no moisture transfer. Current interest in regenerative heat and mass exchangers, which transfer heat and moisture simultaneously [4, 5], has resulted in an extension of the classical definition of heat exchanger effectiveness to exchangers that transfer sensible, latent and total energy. The definition of sensible, latent and total (or enthalpy) effectiveness can be found in several testing standards [6–8] and research papers [9, 10]. For a constant specific heat and heat of phase change, the effectiveness can be defined as:

$$\varepsilon = \frac{\dot{m}(\chi_i - \chi_o)|_s}{\dot{m}_{min}(\chi_{s,i} - \chi_{e,i})} = \frac{\dot{m}(\chi_i - \chi_o)|_e}{\dot{m}_{min}(\chi_{s,i} - \chi_{e,i})} \quad (1)$$

where $\dot{m}$ is the mass flow rate of dry air and χ represents temperature, humidity ratio and enthalpy for sensible (ε_s), latent (ε_l) and total effectivenesses (ε_t) respectively. In equation (1), subscripts i, o, s and e represent the inlet, outlet, supply and exhaust sides of the heat exchanger.

Contrary to the classical definition of heat exchanger effectiveness, the denominator in equation (1) does not represent the thermodynamic maximum energy transfer. As a result, all three effectivenesses can have values below 0 and greater than 1 during simultaneous heat and moisture transfer for some operating conditions. A negative value for latent (or moisture) effectiveness has long been accepted for desiccant dehumidifiers [11, 12]. Therefore, it is not surprising that recent extensive experimental and theoretical research on energy wheels has revealed effectiveness values below 0 and greater than 1 for energy wheels operating under conditions where the sensible, latent or total energy transfer rates are small [13–15]. Despite these weaknesses in the definition of sensible, latent and total effectivenesses, they are currently applied to design applications of energy wheels for any operating condition since they are well known to heat and energy exchanger designers and because there are no practical alternatives. Consequently, equation (1) is the definition of effectiveness used in this paper except that the average of the supply and exhaust side effectiveness is used to increase the accuracy of the results as proposed by Ciepliski et al. [15].

Energy saving and operational benefits of energy wheels have been pointed out by Rengarajan et al. [16] and Shirey and Rengarajan [17] for large and small office buildings in Florida. In these research papers, constant and equal sensible and latent effectivenesses were used to investigate design applications of each energy wheel. Clearly, the economics of energy wheels will strongly depend on their effectiveness and, because there are three different values (i.e. sensible, latent and total) for each operating condition, extensive correlations are needed to allow engineers and designers to quantify energy wheel performance.

Stiesch et al. [11] correlated sensible and total effectivenesses, as a function of temperature, number of transfer units and dimensionless wheel speed using results generated with a numerical model developed by Maclaine-cross [18]. These correlations, although accurate for heating applications, do not appear to account for effectiveness changes that result from changes in the operating condition factor (H^*) developed in Part I of this paper. Simonson et al. [19] show that all three effectiveness values tend to decrease as the supply inlet relative humidity increases (i.e. H^* increases) for warm operating conditions and an energy wheel coated with a molecular sieve desiccant. Unlike heat exchangers that transfer only sensible heat and have effectivenesses that are only a weak function of the temperature and humidity operating conditions, energy wheel effectiveness values depend strongly on the operating conditions as well as their design. These effects must be included in accurate effectiveness correlations.

The purpose of this paper (Part II) is to correlate effectiveness as a function of the dimensionless groups developed in Part I [4]. The importance of certain parameters in the dimensionless groups will be illustrated and the correlations will be used to calculate the effectiveness of an energy wheel with different operating conditions. These effectiveness correlations can be used by manufacturers and HVAC engineers to simply, yet accurately, predict the performance and life cycle cost savings of energy wheels in HVAC systems.

2. Numerical model

Frequently engineering correlations are based on measured data; however, in some cases due to lack of a large range of accurate experimental data for all operating parameters, numerical models are used to simulate data that is then correlated into functional relationships for convenient engineering design. This can be done when the numerical model has been validated with an adequate range of experimental data and with sensitivity studies.

This approach has been adopted in the past for regenerative heat (and mass) exchangers [11, 20, 21] and is the method used in this paper.

The numerical model that has been presented by Simonson and Besant [4, 22] is used in this paper to generate the numerical results that are analyzed to obtain the effectiveness correlations. Validation of the model with experimental data for outdoor temperatures from -20 to 40°C and humidities as high as 90% has been done by Simonson et al. [13, 14]. Simonson and Besant [23] further verify the model by studying several simplifying assumptions and show the importance of each assumption through sensitivity studies.

The general governing equations, summarized in Part I of this paper and detailed by Simonson and Besant [4], are discretized using an implicit finite volume method with a staggered grid. The general dimensional governing equations are used to generate the numerical data rather than the simplified dimensionless ones, developed in Part I, so that the numerical results are unaffected by simplifications made in developing the dimensionless groups. In addition to the approximations made in developing the governing equations, storage in the air (or carry over) is assumed negligible and constant convective heat and moisture transfer coefficients are used. These approximations are expected to change the effectiveness by typically less than 2% [23]. Axial heat conduction in the wheel is neglected (i.e. $k_m \neq 0$) but can be treated by methods presented in Shah [21, 24]. The upwind differencing scheme is used for the air and the central differencing scheme is used for the matrix. The discrete equations are solved using a Gauss–Seidel iteration technique with under relaxation and, to speed up convergence, the energy equation in the matrix is solved using the Tridiagonal Matrix Algorithm [25]. All the simulations in this paper are performed with a grid size of 0.001 m and a time step of 0.01 s. The numerical inaccuracy for these grid and time step sizes is expected to be less than $\pm 0.5\%$ for effectiveness [23]. Also, all simulations use balanced mass flow rates (i.e. $\dot{m}_s = \dot{m}_e$). Simulated and experimental data together with effectiveness correlations for unbalanced flow rates are presented by Simonson et al. [26].

3. Sensitivity of dimensionless groups

In this section, the importance of the dimensionless groups for heat and moisture transfer are shown through sensitivity studies. The effect of the sorption curve and the operating condition factor (H^*) as well as the operating temperature and relative humidity will be studied for the wheel parameters given in Table 1. The effect of individual dimensional parameters such as mass flow rate, surface area, wheel mass and wheel speed will also be examined. The sorption curve used in the simulation is a general sorption curve,

$$u = \frac{Wm}{1 - C + C/\phi} \tag{2}$$

where Wm represents the maximum moisture content of the desiccant and C determines the type of desiccant. Several desiccant coatings, such as molecular sieve, silica gel, activated alumina and activated carbon, have sorption characteristics that can be modeled using equation (2).

Table 1
Energy wheel parameters used in the sensitivity studies

Wheel no.	NTU_o	Cr_o^*	Crm_o^*
1	10	10	10
2	5	5	5
3	3	3	3

3.1. Effect of sorption curve on latent effectiveness

The storage of moisture in the desiccant ($Cr^*_{mt,o}$) depends on the slope of the sorption curve as can be seen in the following equation,

$$Cr^*_{mt,o} = (Crm^*_o)\left.\frac{\partial u}{\partial \phi}\right|_{\phi_{ave}} \left(\frac{e^{\left(\frac{5294}{T_{ave}}\right)}}{10^6} - 1.61\phi_{ave} \right) \tag{3}$$

where:

$$Crm^*_o = \frac{M_{d,dry}N}{\dot{m}_{min}}, \quad \text{and} \tag{4}$$

T_{ave} is $(T_{s,i} + T_{e,i})/2$ in K and ϕ_{ave} is $(\phi_{s,i} + \phi_{e,i})/2$. It is expected that $Cr^*_{mt,o}$ will be proportional to the slope of the sorption curve at the average operating humidity. Therefore, to see if the latent effectiveness changes as expected with changes in the slope of the sorption curve, simulations with constant exhaust conditions (24°C and 50% RH) and various supply relative humidities and constant supply temperature of 35°C are given in Fig. 1 for the three wheels listed in Table 1 with various sorption curve constants (C). Wm is also varied in Fig. 1.

The results in Fig. 1 show a wide range of effectiveness values for the different wheels with different sorption curves and supply inlet humidities. To help explain the results in Fig. 1, the sorption curves and slope of the sorption curve are presented in Fig. 2.

The results in Fig. 1 clearly show that the slope of the sorption curve influences the latent effectiveness, particularly for wheel 3 which has low values of NTU_o, Cr_o^* and Crm_o^*. The effectiveness for the linear sorption curve ($C = 1$) has the highest values and is nearly constant with

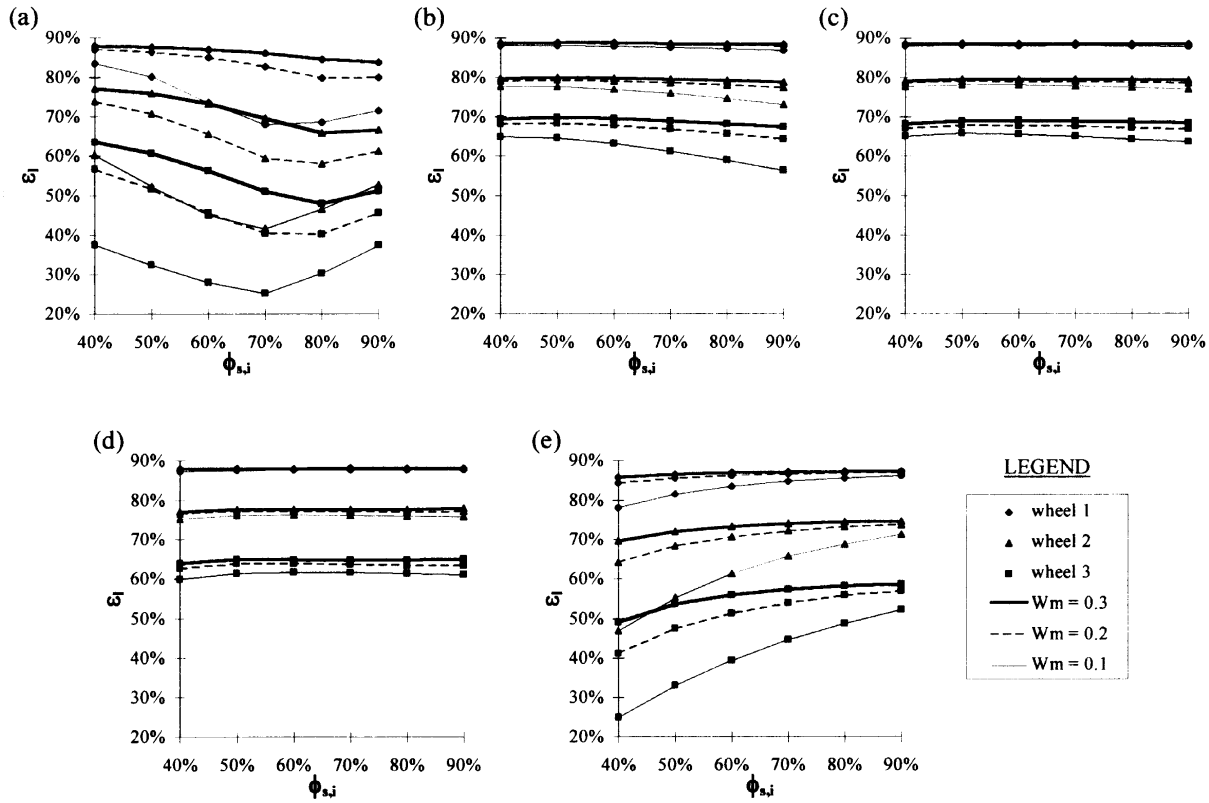

Fig. 1. Variation in latent effectiveness with supply inlet humidity for different energy wheels and sorption curve constants: (a) $C = 0.01$, (b) $C = 0.1$, (c) $C = 1$, (d) $C = 10$ and (e) $C = 100$ with $T_{e,i} = 24°C$, $\phi_{e,i} = 50\%$ and $T_{s,i} = 35°C$.

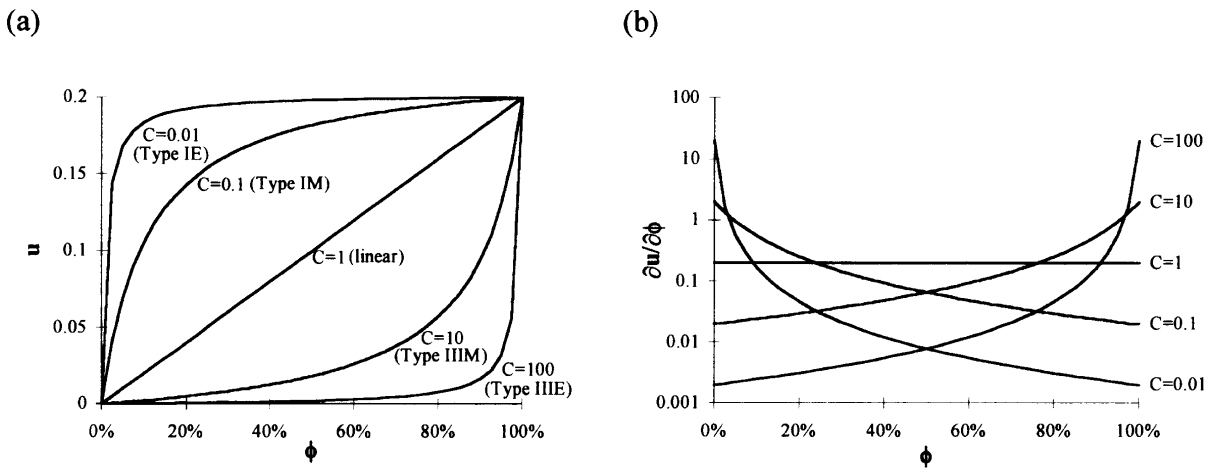

Fig. 2. The (a) sorption curve and (b) slope of the sorption curve for $Wm = 0.2$.

changing humidity because the slope of the sorption curve is constant.

Figure 1(a) shows that a wheel coated with a Type I extreme (Type IE) desiccant (i.e. $C = 0.01$) will have a high effectiveness at lower supply inlet relative humidities but ε_l decreases as ϕ increases. This result can be explained from equation (3) and Fig. 2 because the slope of a Type I extreme sorption curve is high for low values

of ϕ and decreases as ϕ increases. The change in effectiveness is particularly large for wheel 3 which has a low value of Crm^*_o. This trend of increasing sensitivity of $Cr^*_{mt,o}$ for lower value of $Cr^*_{mt,o}$ is the same as for regenerative sensible heat exchangers (see Part I, fig. 2). At about 70% relative humidity, ε_l begins to increase with increasing ϕ for a Type IE sorption curve (i.e. a molecular sieve desiccant coating) because saturation conditions begin at this humidity as shown by Simonson et al. [19]. As discussed in section 3.4 of Part I and Simonson and Besant [22], ε_l increases with increasing ϕ during saturation conditions. Equation (3) does predict this because it represents the dimensionless moisture storage capacity of the matrix during sorption conditions only.

The effectiveness of a wheel with a Type III extreme (Type IIIE) desiccant (i.e. $C = 100$) is opposite to one with a Type IE desiccant. As ϕ increases for this case, ε_l increases because the slope of the sorption curve increases with increasing ϕ. The results predicted with Type I and III moderate sorption curves are similar to those for their respective extreme sorption curves except that the change in ε_l is much smaller because the slope of the sorption curve changes less dramatically with ϕ.

The results in Fig. 1 show that a linear sorption curve has the highest effectiveness over a typical range of operating conditions. Figure 2(b) shows that this is due to the steep slope of the linear sorption curve over the range $25 < \phi < 75\%$. This type of desiccant (e.g. silica gel) is therefore recommended for most air conditioning energy recovery applications where both sensible and latent energy transfer occur. As a result, the linear sorption curve will be used for simulations in the rest of this paper unless specified otherwise. An additional advantage of silica gels is that they have high moisture capacities, typically 40% by mass (i.e. $Wm = 0.4$). This will further increase ε_l as can be seen in Fig. 1.

Desiccant dryers, which are intended to transfer water vapor, are very different than energy wheels. The reason why a Type 1M desiccant has been recommended for desiccant dryers by several researchers [12, 27] is now apparent when Figs 1 and 2 are examined together with equation (3). The inlet conditions to a desiccant dryer are typically 90°C and 3–5% RH for regeneration and 35°C and 40–45% RH for air drying, giving an average operating humidity in the desiccant dryer wheel of 20–25%. At this humidity, the Type 1M sorption curve has the largest slope (see Fig. 2(b)) and therefore would be expected to perform the best for these operating conditions. Clearly, $Cr^*_{mt,o}$ is essential to understand changes in ε_l caused by changes in the sorption curve and inlet humidity for both desiccant dryers and energy wheels.

3.2. Effect of temperature on latent effectiveness

The storage of moisture in the desiccant ($Cr^*_{mt,o}$) depends on the operating temperature of the energy wheel as indicated in equation (3). Equation (3) shows that $Cr^*_{mt,o}$ and consequently ε_l is expected to decrease as the average operating temperature increases. Figure 3 shows simulations of the variation in latent effectiveness due to changes in the operating temperature with constant exhaust conditions (24°C and 50% RH) and different supply temperatures and a constant supply humidity of 60%.

The results in Fig. 3 suggest that the operating temperature affects the latent energy performance of the energy wheel, especially at high values of inlet temperature. The decrease in ε_l for increasing $T_{s,i}$ is expected from the dimensionless group $Cr^*_{mt,o}$. The decrease in effectiveness is particularly large for wheel 3 which has low values of NTU_o, Cr^*_o and Crm^*_o. Wheels 1 and 2 are less affected by changes in operating temperature because they have higher values of NTU_o, Cr^*_o and Crm^*_o.

3.3. Effect of H* and η on sensible effectiveness

According to the developed dimensionless groups for heat transfer in Part I,

$$NTU_{ht,o} = \frac{NTU_o}{1+\eta\dfrac{\varepsilon_l}{\varepsilon_s}H^*} \quad \text{and} \tag{5}$$

$$Cr^*_{ht,o} = \frac{Cr^*_o}{1+\dfrac{\varepsilon_l}{\varepsilon_s}H^*} \tag{6}$$

where:

$$NTU_o = \frac{hA_s}{(\dot{m}C_{p_a})_{min}} \quad \text{and} \tag{7}$$

$$Cr^*_o = \frac{(MC_p)_m N}{(\dot{m}C_{p_a})_{min}}. \tag{8}$$

Equations (5)–(8) show that the effectiveness of an energy wheel should depend on the operating condition factor (H^*) and the fraction of phase change energy that is delivered directly to the air (η). This is the case as can be seen in Fig. 4 which shows the sensible effectiveness as a function of H^* for the three wheels listed in Table 1 for values of $\eta = 0$ and $\eta = 0.1$. The simulation results in Fig. 4 have exhaust inlet conditions of 24°C and 50% RH and a supply inlet temperature of 27°C.

Figure 4 simulation results show that the sensible effectiveness is dependent on both H^* and η with ε_s being a linear function of H^*. As H^* and/or η increase, ε_s decreases. These results can be explained with equations (5) and (6) which show that both $NTU_{ht,o}$ and $Cr^*_{ht,o}$ decrease as H^* increases, but only $NTU_{ht,o}$ decreases with η. When $H^* = 0$, $NTU_{ht,o} = NTU_o$ and $Cr^*_{ht,o} = Cr^*_o$ and the conventional correlation for sensible regenerative heat exchangers [2, 4, 21] equation (15) is expected to apply. This is found to be the case with the difference between the simulated values and those calculated with

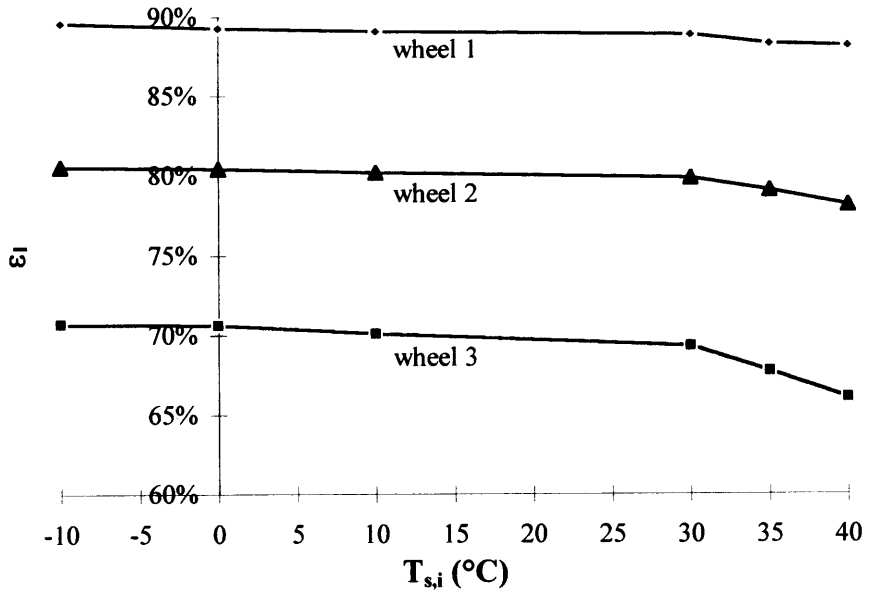

Fig. 3. Latent effectiveness versus supply inlet temperature for the energy wheels in Table 1 with $T_{e,i} = 24°C$, $\phi_{e,i} = 50\%$ and $\phi_{s,i} = 60\%$.

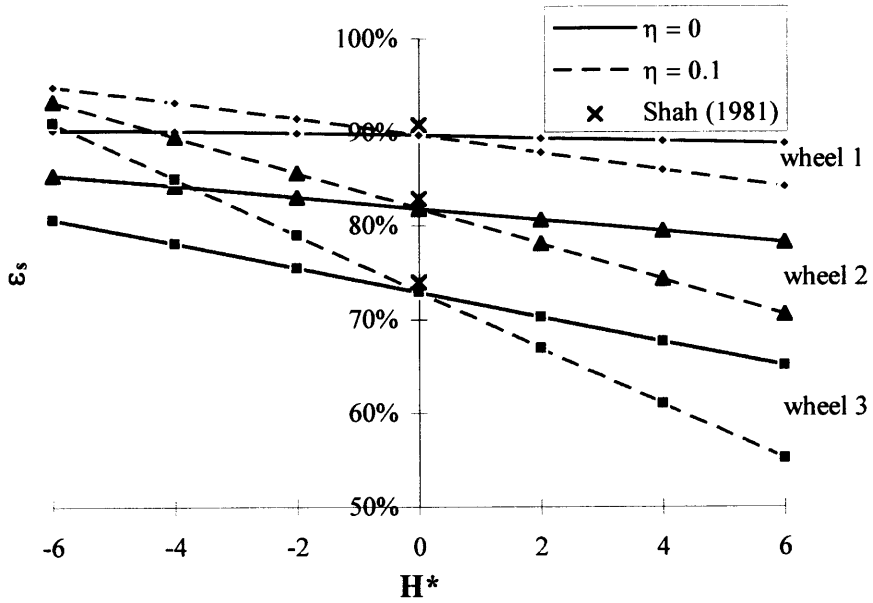

Fig. 4. Effect of H^* and η on the sensible effectiveness of different energy wheels with $T_{e,i} = 24°C$, $\phi_{e,i} = 50\%$ and $T_{s,i} = 27°C$.

the sensible wheel correlation being less than 1%, when $H^* = 0$. Figure 4 indicates that large errors will result if the sensible wheel correlation is applied to operating conditions where moisture transfer is significant. This explains why Simonson and Besant [23] found that during cold operating conditions the sensible effectiveness could be predicted reasonably accurately with the correlation for sensible regenerative heat exchangers, but significant errors occurred when the temperature and humidity were high. Therefore, the solution for sensible heat transfer in regenerative heat exchangers is a special case of the more general solution of simultaneous heat and moisture transfer in energy wheels and applies when $H^* = 0$.

Similar to the previous two sections, Fig. 4 shows that wheel 3 is more sensitive to the operating conditions (i.e.

H^*) and η than wheels 1 and 2. The reason for this is simply that decreasing $NTU_{ht,o}$ and $Cr^*_{ht,o}$ has a larger effect on ε_s when $NTU_{ht,o}$ and $Cr^*_{ht,o}$ are small.

The results in Fig. 4 show a very important characteristic of energy wheels: increasing moisture transfer typically decreases ε_s. For most operating conditions of practical importance, the operating condition factor (H^*) is positive, which means that, if H^* is large and high sensible effectivenesses are sought, wheels with larger values of NTU_o and Cr^*_o must be used because the moisture transfer will decrease the heat transfer.

3.4. *Verification of* NTU_o, Cr^*_o *and* Crm^*_o

The definitions of the dimensionless groups NTU_o $(= hA_a/(\dot{m}C_{p_a})_{min})$, Cr^*_o $(=(MC_p)_m N/(\dot{m}C_{p_a})_{min})$ and Crm^*_o $(= M_d N/\dot{m}_{min})$ each include several dimensional parameters as shown. Since the development of these dimensionless groups involved several approximations (see Part I), it is important to verify that these complete groups affect the effectiveness regardless of the value of the individual dimensional parameters. Figure 5 presents simulation results that show how NTU_o affects ε_s and ε_l when NTU_o is changed numerically by changing the convective heat transfer coefficient (h), the heat and mass transfer surface area (A_s) and the mass flow rate of dry air ($\dot{m}$) from the base parameters shown in Table 2.

It can be seen in Fig. 5 that the effectiveness of the energy wheel is the same at a given value of NTU_o regardless of which dimensional parameter is changed to attain the specific value of NTU_o. In Fig. 5, $Cr^*_o = Crm^*_o =$ constant, therefore when $\dot{m}$ is changed, M_d and M_m are also changed to keep Cr^*_o and Crm^*_o constant. Figure 5 shows that the effect of NTU_o on the sensible and latent effectiveness is similar to that for a counter flow heat exchanger.

Figures 6 and 7 show that Cr^*_o and Crm^*_o affect the effectiveness values in a manner similar to the way Cr^*_o affects the effectiveness of a sensible heat regenerator. Cr^*_o has a larger effect than Crm^*_o. The influence of individual dimensional parameters can clearly be seen to be of secondary importance to the influence of the entire dimensionless group. The greatest difference between the effectiveness calculated with different values of the dimensional parameters but the same values of NTU_o, Cr^*_o and Crm^*_o is 0.3%. This shows that these dimensionless groups are applicable to energy wheels. It is also interesting to note that Cr^*_o and Crm^*_o affect both ε_s and ε_l which shows that the storage of heat and moisture in the energy wheel are coupled. This coupling must be accounted for in the effectiveness correlations.

4. Effectiveness correlations

In this section, the correlations for sensible, latent and total effectiveness with balanced flow rates ($C^* = 1$) are presented. (Correlations for unbalanced flow rates are presented by Simonson et al. [26].) In each case the dimensionless groups are used to fit simulation data with a correlation that has a similar form as the effectiveness correlation for a sensible rotary heat exchanger. An equation of this form is used because the governing equations for energy wheels and sensible regenerators are of the same form and therefore the solutions to the governing equations are expected to be similar. The agreement between the correlations and simulation data is nearly as good as that presented by Shah [21, 24] despite the fact

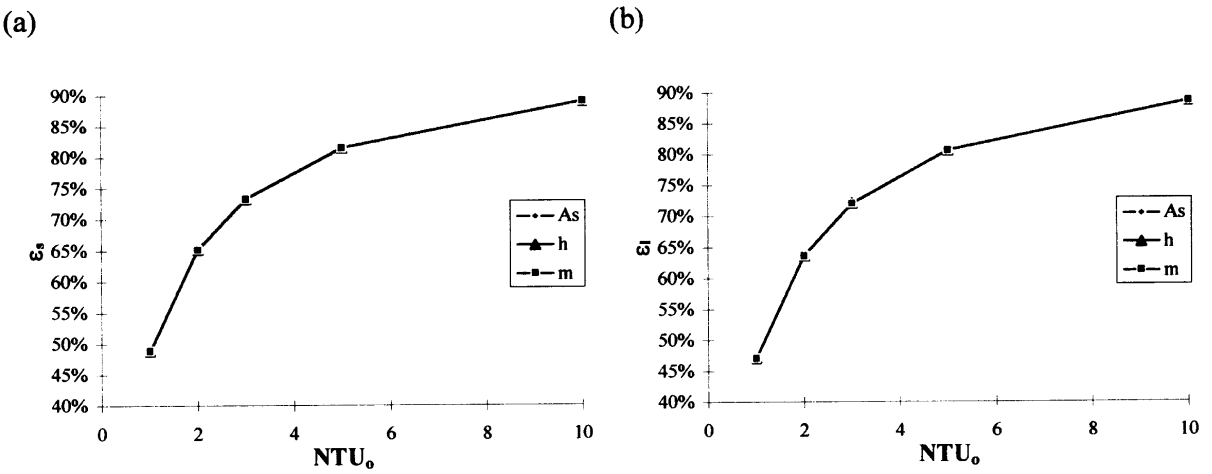

Fig. 5. Effect of NTU_o on (a) ε_s and (b) ε_l. NTU_o is changed by changing h, A_s and $\dot{m}$ with $T_{e,i} = 24°C$, $\phi_{e,i} = 50\%$ and $T_{s,i} = 35°C$, $\phi_{s,i} = 60\%$.

Table 2
Energy wheel base parameters used to study the sensitivity of each dimensional parameter

h [W m^{-2} K^{-1}]	A_s [m^2]	$\dot{m}$ [kg s^{-1}]	N [cycles s^{-1}]	$(M\,C_p)_m$ [J kg^{-1} K^{-1}]	M_d [kg]
40	252	0.5	1/3	15 120	15

($NTU_o = Cr^*_o = Crm^*_o = 10$)

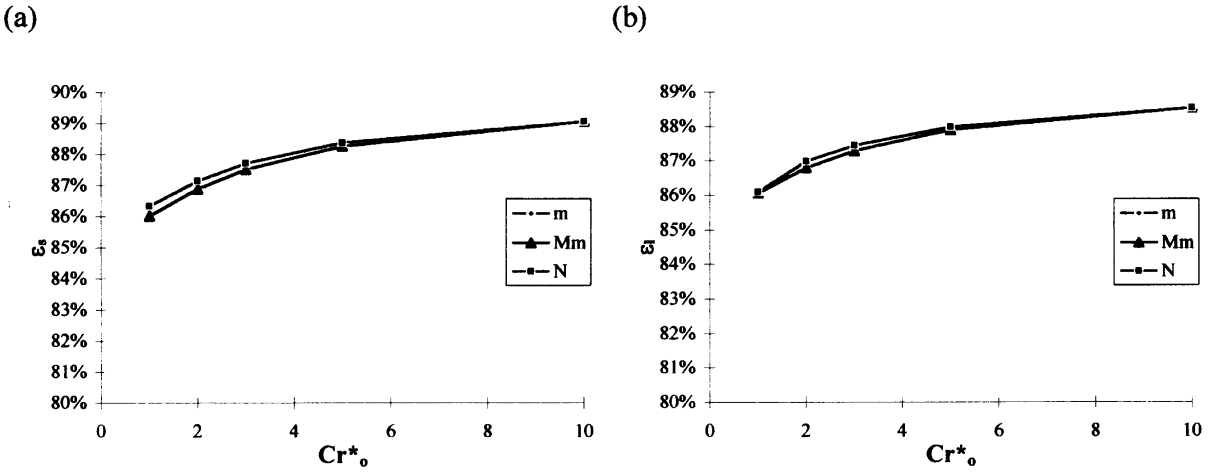

Fig. 6. Effect of Cr^*_o on (a) ε_s and (b) ε_l. Cr^*_o is changed by changing M_m, N and $\dot{m}$ with $T_{e,i} = 24°C$, $\phi_{e,i} = 50\%$ and $T_{s,i} = 35°C$, $\phi_{s,i} = 60\%$.

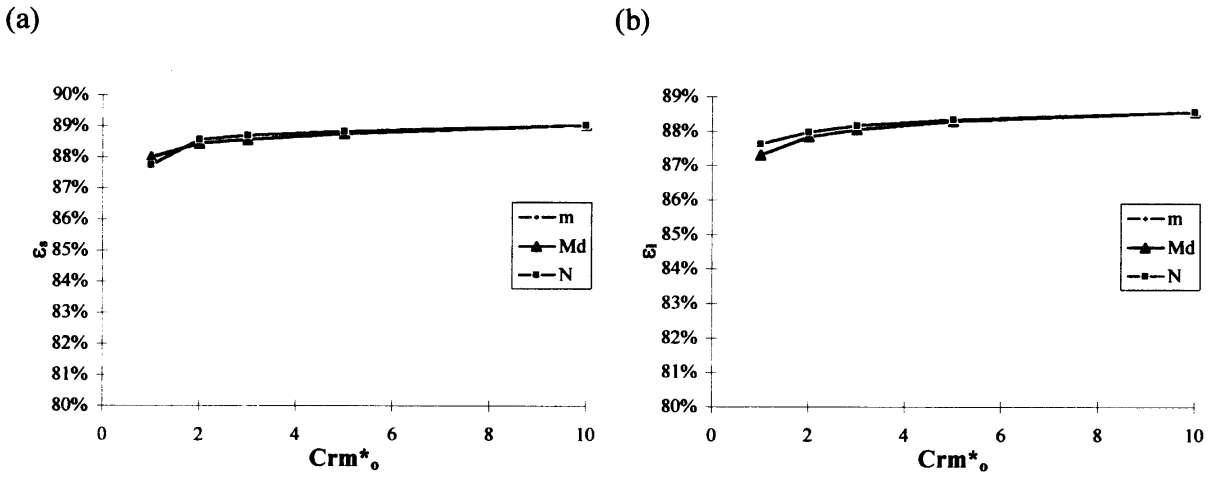

Fig. 7. Effect of Crm^*_o on (a) ε_s and (b) ε_l. Crm^*_o is changed by changing M_d, N and $\dot{m}$ with $T_{e,i} = 24°C$, $\phi_{e,i} = 50\%$ and $T_{s,i} = 35°C$, $\phi_{s,i} = 60\%$.

that the number of variables is larger and several simplifications and approximations have been made in determining the dimensionless groups. Although the dimensionless variables developed in Part I are shown to have physical significance, we have chosen only the dimensionless components of $NTU_{ht,o}$ and $Cr^*_{ht,o}$ for the sensible effectiveness correlation. Correlations of ε_s with $NTU_{ht,o}$ and $Cr^*_{ht,o}$ explicitly formulated proved to be slightly less

accurate and for a narrower range of variables than the ones finally presented. Furthermore, ε_s and ε_l can be calculated independently with the selected correlations, eliminating the need for an iterative solution. The correlations presented in this section were determined by minimizing the maximum difference between over 600 simulated effectiveness values and those predicted by the correlation. The coefficients of the correlation were determined using an optimization routine in a commercially available spreadsheet package.

4.1. Latent effectiveness

The correlation for latent effectiveness is determined from the over 600 simulation data points shown in Fig. 8 which cover a range of temperatures from -20 to 40°C and relative humidities near 0 to 90% ($-6 \leqslant H^* \leqslant 6$). Simulation data points with H^* in the range of $-0.3 \leqslant H^* \leqslant 0.2$ have been eliminated because ε_l can be quite large (>100%) or small (<20%) in this range [15]. Condensation and frosting effects have also been eliminated. The maximum difference between simulated and correlated effectiveness is 2% with 98% of the data agreeing within $\pm 1.5\%$. The correlation for latent effectiveness is:

$$\varepsilon_l = \frac{NTU_o}{1+NTU_o}\left(1-\frac{1}{0.54(Cr^*_{mt,o})^{0.86}}\right) \times\left(1-\frac{1}{(NTU_o)^{0.51}(Cr^*_{mt,o})^{0.54}H^*}\right) \quad (9a)$$

where:

$$Cr^*_{mt,o} = (Crm^*_o)^{0.58}\,Wm^{0.33}\left(\left.\frac{\partial u}{\partial\phi}\right|_{\phi_{ave}}\right)^{0.2} \times (Cr^*_o)^{1.13}\left(\frac{e^{\left(\frac{1482}{T_{ave}}\right)}}{47.9}-1.26(\phi_{ave})^{0.5}\right)^{4.66}. \quad (9b)$$

Equations (9a) and (9b) are for a linear sorption curve with: $2 \leqslant NTU_o \leqslant 10$, $3 \leqslant Cr^*_o \leqslant 10$, a full range of Crm^*_o, $-0.3 > H^* > 0.2$, $0.1 \geqslant Wm \geqslant 0.5$ and $C^* = 1.0$. For $-0.3 \leqslant H^* \leqslant 0.2$, the moisture transfer can be neglected for most air conditioning energy recovery applications because the amount of moisture transferred during these operating conditions is small. It should be noted that for a linear sorption curve the slope of the sorption curve ($\partial u/\partial\phi$) is constant and equal to Wm. Equation (9) can also be used for desiccants with Type IM for Type IIIM sorption curves (i.e. $10 \geqslant C \geqslant 0.1$) but the uncertainty is expected to increase to about $\pm 5\%$. The cor-

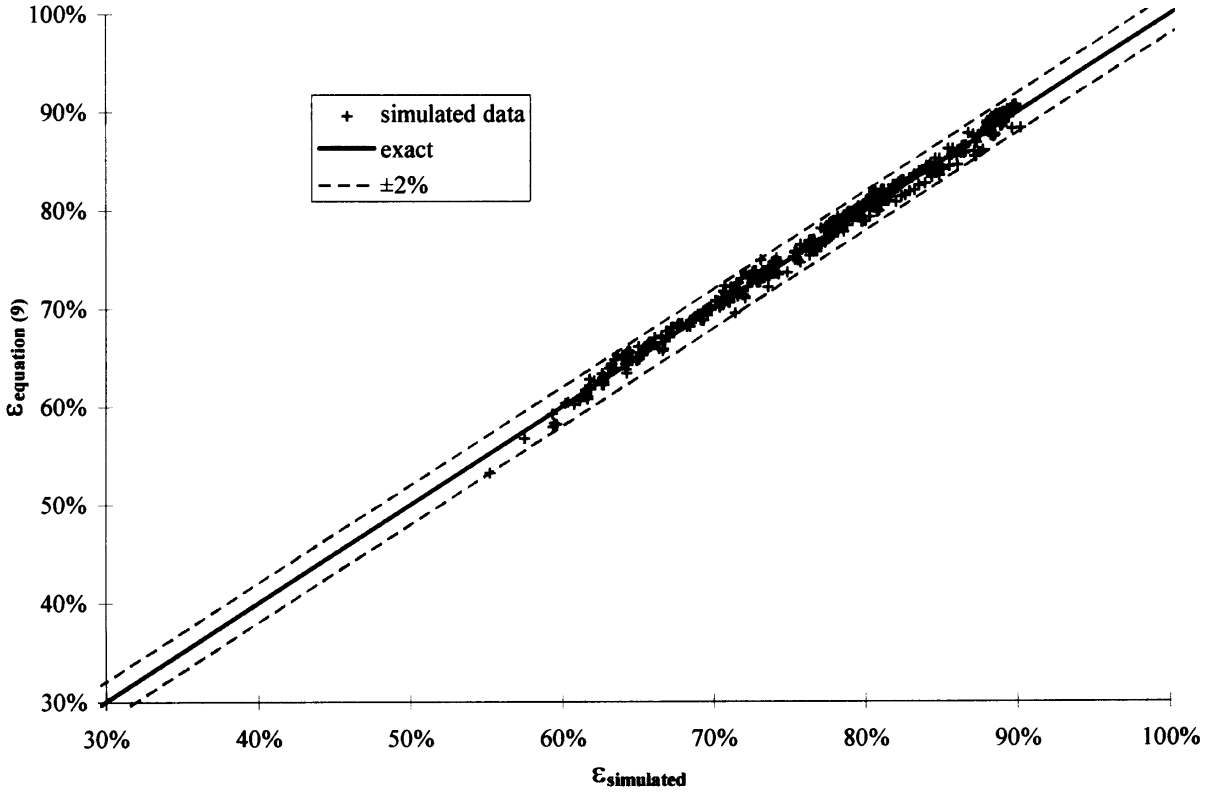

Fig. 8. Latent effectiveness calculated with equation (9) compared to the simulated latent effectiveness.

relation in equation (9) is intended to apply for $0 \leqslant \varepsilon_l \leqslant 100\%$.

4.2. Sensible effectiveness

The correlation for sensible effectiveness is proposed in the following format,

$$\varepsilon_s = \varepsilon_{s(H^*=0)} - \Delta\varepsilon_s \tag{10}$$

where $\Delta\varepsilon_s$ is a function of H^*, η, NTU_o, Cr_o^* and Crm_o^* and Wm. $\varepsilon_{s(H^*=0)}$ is the effectiveness of a sensible wheel (i.e. no moisture transfer) and $\Delta\varepsilon_s$ is a factor which adjusts this effectiveness to account for the effects of moisture transfer. A relation of this type is chosen because $\varepsilon_{s(H^*=0)}$ is well known and $\Delta\varepsilon_s$ is a linear function of H^* (see Fig. 4). Figure 9 contains $\Delta\varepsilon_s$ for $H^* = 6$, $\eta = 0.1$, $Wm = 0.2$ and $Cr_o^*/Crm_o^* = 5$ with various values of NTU_o and Cr_o^* and shows that $\Delta\varepsilon_s$ can be quite large for low value of Cr_o^*. For example, with $NTU_o = 10$ and $Cr_o^* = 2$, $\Delta\varepsilon_s = 50\%$. $\Delta\varepsilon_s$ is less than 25% for $Cr_o^* \geqslant 3$ and therefore the correlations in this paper use this limit.

The final sensible effectiveness correlation is:

$$\varepsilon_s = \frac{NTU_o}{1+NTU_o}\left(1-\frac{1}{7.5Cr_o^*}\right) - \left[\frac{0.26\left(\dfrac{Cr_o^*}{Wm^2Crm_o^*}\right)^{0.28}}{7.2(Cr_o^*)^{1.53}+\dfrac{210}{(NTU_o)^{2.9}}-52} + \frac{0.31\eta}{(NTU_o)^{0.68}}\right] H^*. \tag{11}$$

Equation (11) agrees with the over 600 simulated data points in Fig. 10 within $\pm 2.5\%$ (98% of data within $\pm 2\%$) for the following range of parameters: $0 \leqslant \eta \leqslant 0.1$, $-6 \leqslant H^* \leqslant 6$, $2 \leqslant NTU_i \leqslant 10$, $3 \leqslant Cr_o^* \leqslant 10$, $1 \leqslant Cr_o^*/Crm_o^* \leqslant 5$, $0.1 \leqslant Wm \leqslant 0.5$, $C = 1$ and $C^* = 1$. The uncertainty in equation (11) increases to $\pm 3\%$ for $0.1 \leqslant C \leqslant 1$ and $\pm 5\%$ for $0.1 \leqslant C \leqslant 10$. Even though equation (11) predicts the simulated effectiveness well for $\varepsilon_s > 100\%$, it is intended to be used for $0 \leqslant \varepsilon_s \leqslant 100\%$.

Equation (11) is for negligible axial heat conduction through the matrix of the energy wheel. Simulation results show that the axial conduction can be accounted for by the method in Shah [21, 24] with little loss in accuracy. The correction for axial thermal conduction is [24],

$$\varepsilon_{s_{(k_m\neq 0)}} = \varepsilon_{s_{(k_m=0)}} C_\lambda \tag{12}$$

where:

$$C_\lambda = \frac{1+NTU_o}{NTU_o}\left[1-\frac{1}{1+NTU_o\dfrac{1+\lambda\Phi}{1+\lambda NTU_o}}\right] \tag{13}$$

$$\lambda = \frac{A_m k_m}{L(\dot{m}C_{p_a})_{min}}, \quad \text{and} \tag{14}$$

$$\Phi = \sqrt{\frac{\lambda NTU_o}{1+\lambda NTU_o}}\tanh\left[\frac{NTU_o}{\sqrt{\dfrac{\lambda NTU_o}{1+\lambda NTU_o}}}\right]$$

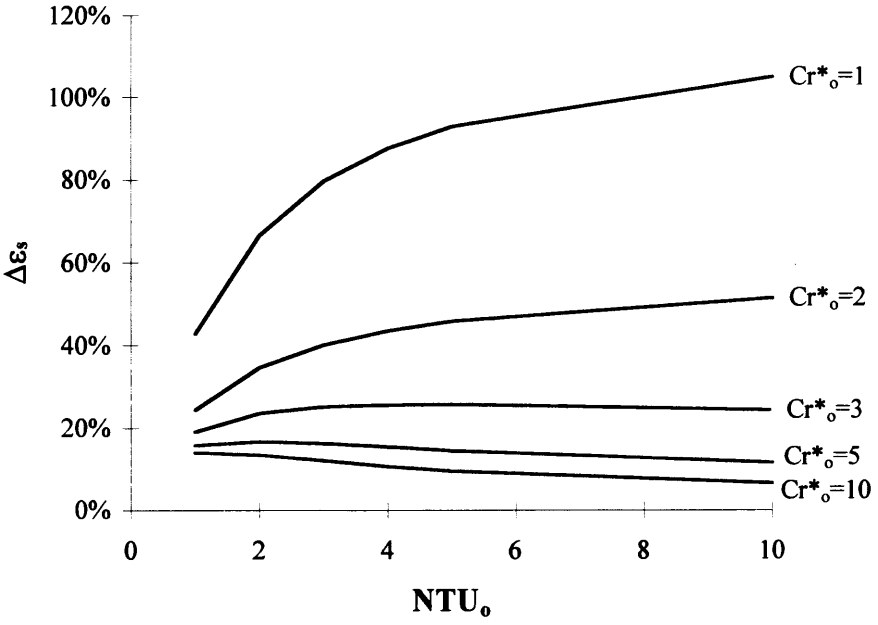

Fig. 9. $\Delta\varepsilon_s$ as a function of NTU_o, Cr_o^* for $H^* = 6$, $\eta = 0.1$, $Wm = 0.2$ and $Cr_o^*/Crm_o^* = 5$.

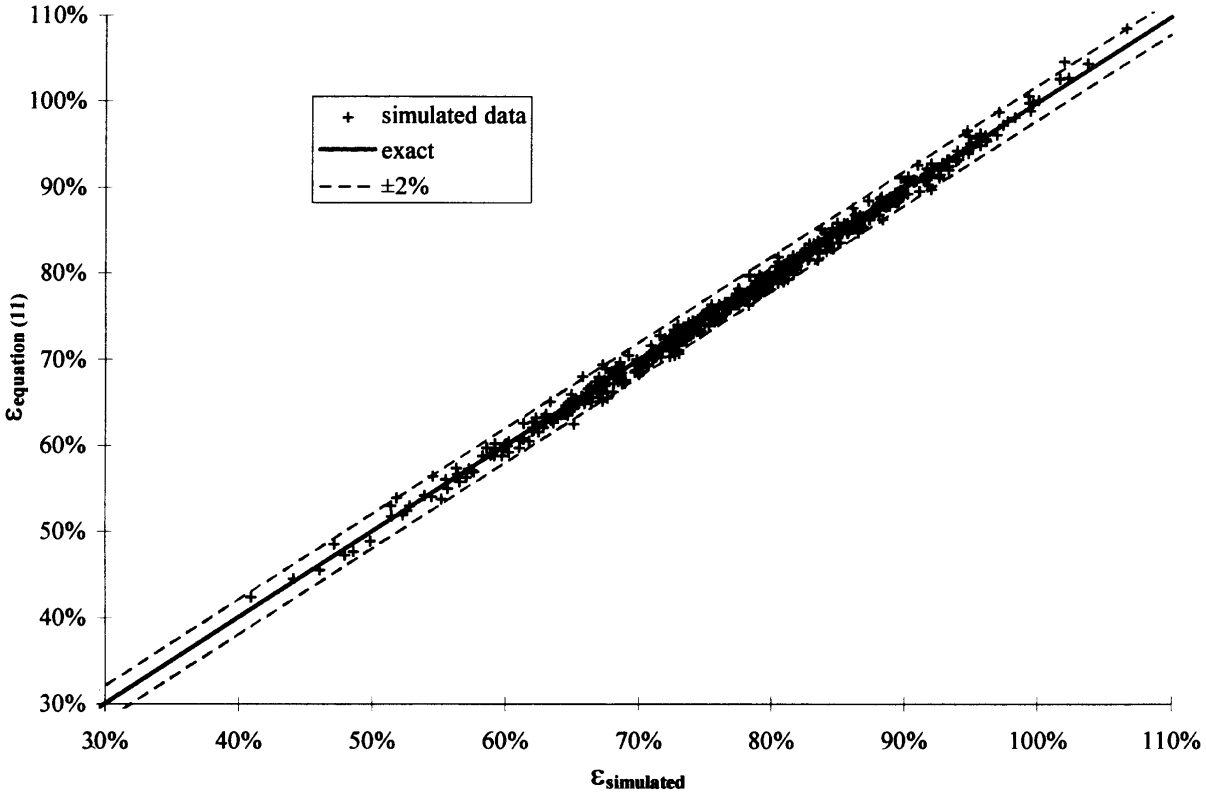

Fig. 10. Sensible effectiveness calculated with equation (11) compared to the simulated sensible effectiveness.

$$\approx \sqrt{\frac{\lambda NTU_o}{1+\lambda NTU_o}} \quad \text{for } NTU_o \geqslant 3. \tag{15}$$

4.3. Total effectiveness

Using the simulated values for ε_s and ε_l in the relation,

$$\varepsilon_t = \frac{\varepsilon_s + \varepsilon_l H^*}{1+H^*} \tag{16}$$

gives values for ε_t that are less than 0.4% different from those simulated for the over 600 data points in Figs 9 and 10 when $-1.5 > H^* > -0.5$. Data points in the range of $-1.5 \leqslant H^* \leqslant -0.5$ have been eliminated because ε_t is discontinuous at $H^* = -1$. If the correlated values of ε_s (equation (11)) and ε_l (equation (9)) are used in equation (16), the uncertainty in ε_t is expected to be the same as that quoted for equations (9) and (11) (i.e. $\pm 2.5\%$).

5. Illustrative example

The illustrative example in this paper is for the rating of an energy wheel rather than sizing each component of a wheel. The objective of the rating problem is to verify the thermal and mass transfer performance of an existing energy wheel as specified by the manufacturer or to determine the off-design performance. Many details of the methodology for the rating and sizing problems are given in Shah [24] for sensible rotary heat exchangers. The basic procedure is the same for energy wheels with the main difference being that more property data and more complex equations are required to calculate the energy wheel performance. In this example, the somewhat hypothetical energy wheel with the properties listed in Table 3, operating in the conditions listed in Table 4 will be considered. The value of the dimensionless groups and the effectiveness values at the illustrative hot and cold test conditions are also given in Table 4. In each case the effectiveness correlations (i.e. equations (9), (11), (12) and (16)) are used to calculate the effectiveness values which include axial conduction through the wheel. In all cases $\eta = 0.05$.

5.1. Mass flow rate of air

Figure 11 shows the effect of mass flow rate on the sensible, latent and total effectiveness of the energy wheel

Table 3
Property data of the energy wheel

	Entire wheel	
$D = 1$ m	$L = 0.1$ m	$N = 1/3$ cycles s^{-1} (20 rpm)
$M_m = 14$ kg	$\beta = 2667$ m^2/m^3	porosity = 0.80
	Individual tube (sine duct)	
$D_h = 1.2 \times 10^{-3}$ m	$a^* = 0.4$	$Nu = 2.46$ [28]
	Desiccant (silica gel @ 20% by mass)	
$Wm = 0.4$	$C = 1$	$\sigma_d = 0.68$
$\rho_d = 350$ kg m^{-3}	$C_{p_d} = 615$ J kg^{-1} K^{-1}	$k_d = 0.06$ W m^{-1} K^{-1}
	Support material (aluminum)	
$\rho_{sup} = 2702$ kg m^{-3}	$C_{p_{sup}} = 903$ J kg^{-1} K^{-1}	$k_{sup} = 237$ W m^{-1} K^{-1}

Table 4
Design operating conditions, dimensionless groups and effectiveness of the energy wheel

Hot test	$T_{s,i} = 30°C$	$\phi_{s,i} = 50\%$
$\dot{m}_s = \dot{m}_e = 0.6$ kg s^{-1}	$T_{e,i} = 24°C$	$\phi_{e,i} = 50\%$
$H^* = 1.67$	$NTU_o = 4.6$	$Cr_o^* = 6.5$
$Crm_o^* = 1.6$	$C_\lambda = 0.892$	$Cr_{mt,o}^* = 174.3$
$\varepsilon_s = 70.3\%$	$\varepsilon_l = 79.1\%$	$\varepsilon_t = 75.8\%$
Cold test	$T_{s,i} = 24°C$	$\phi_{s,i} = 50\%$
$\dot{m}_s = \dot{m}_e = 0.6$ kg s^{-1}	$T_{e,i} = -10°C$	$\phi_{e,i} = 50\%$
$H^* = 0.63$	$NTU_o = 4.6$	$Cr_o^* = 6.5$
$Crm_o^* = 1.6$	$C_\lambda = 0.892$	$Cr_{mt,o}^* = 1599$
$\varepsilon_s = 71.2\%$	$\varepsilon_l = 80.9\%$	$\varepsilon_t = 74.9\%$

for the hot and cold test conditions. The decreasing effectiveness with increasing mass flow rate (or face velocity) is expected. Effectiveness is more sensitive to mass flow rate changes for the hot test than for the cold test.

5.2. Wheel speed

Changing the wheel speed of the energy wheel will reduce Cr_o^* and Crm_o^* and consequently the effectiveness. This is shown in Fig. 12 where the effectiveness is plotted as a function of wheel speed. Although the effectiveness correlations were limited to $Cr_o^* \geqslant 3$, the results in Fig. 12 appear reasonable for $Cr_o^* \geqslant 1$. The differences between simulated and calculated effectiveness values for $N = 5$ rpm are less than 5% which is smaller than the changes in effectiveness that are seen in Fig. 12. It would appear from this example that using wheel speed to control the rate of heat and moisture transfer for air conditioning applications would likely lead to space temperature and humidity problems. This has been observed in practice.

5.3. Operating condition factor (H*)

The correlations can also be used to show the effect of the operating temperature and humidity on the effectiveness of the energy wheel described in Tables 3 and 4 (Fig. 13). The results in Fig. 13 are for the hot test conditions with various supply inlet relative humidities and they show the sensitivity of effectiveness to the operating conditions (H^*). In particular, ε_l is discontinuous at $H^* = 0$ with $\varepsilon_l \to +\infty$ as $H^* \to 0^-$. The total effectiveness is also discontinuous with the discontinuity occurring at $H^* = -1$ which corresponds to the case of equal inlet enthalpies to the energy wheel. For $H^* \approx 0$ and $H^* \approx -1$, the moisture transfer and energy transfer rates of the energy wheel are respectively small and therefore these operating conditions are not important for energy saving calculations and optimization of air conditioning designs using energy wheels. Figure 13 shows that axial conduction through the aluminum support material of the energy wheel reduces the effectiveness of the energy wheel by 9% for these operating conditions.

The brief application of the effectiveness correlations given in this paper display their utility. These correlations are much simpler to use than detailed simulations programs which are the current alternative. The correlations are especially important because they can be easily implemented into entire building simulation programs which will allow life cycle cost and energy saving studies. These correlations will also permit HVAC engineers to more accurately design and predict savings for energy wheels.

6. Conclusions

Simulation and correlation results presented in this paper show the importance of operating conditions on the effectiveness of an energy wheel. The operating con-

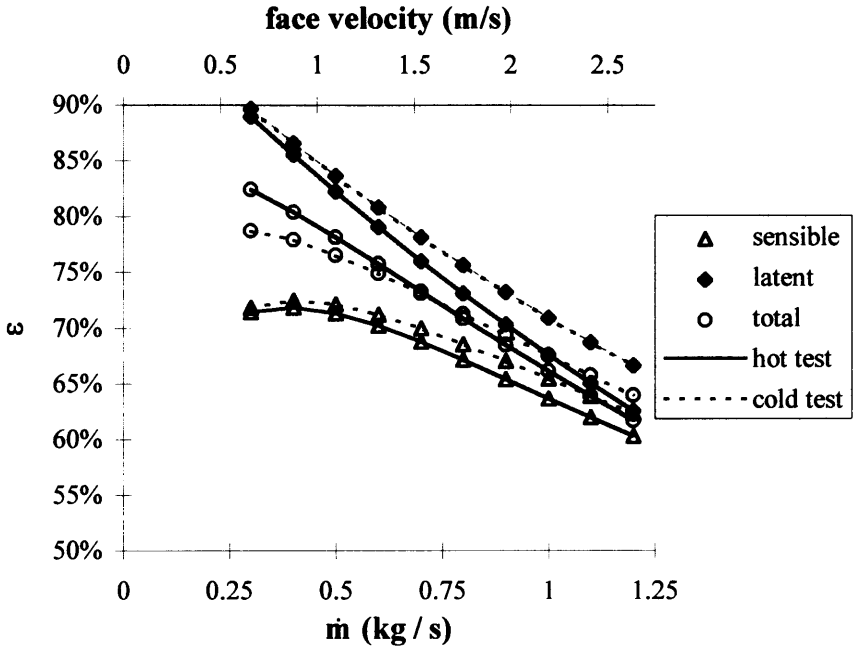

Fig. 11. Effectiveness versus mass flow rate for balanced supply and exhaust mass flow rates.

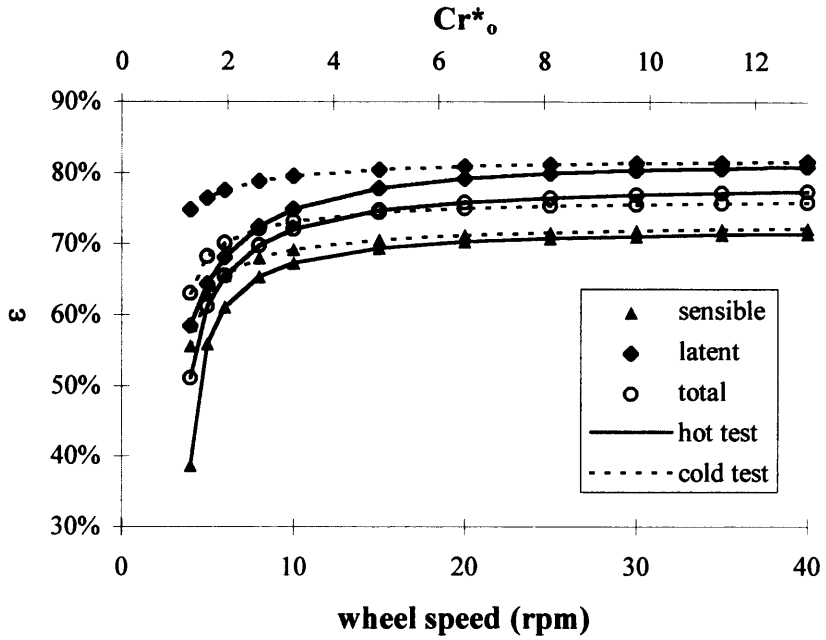

Fig. 12. Effectiveness versus wheel speed for balanced mass flow rates.

ditions have the largest effect on the effectiveness when the traditional value of NTU_o and Cr_o^* and the newly defined Crm_o^* (which is similar to Cr_o^* except that it applies to moisture storage rather than energy storage) are low. Changes in effectiveness that result from changes in the operating conditions and sorption curve can be explained by the dimensionless groups.

The dimensionless groups and simulation results show that a desiccant with a linear sorption curve will have the best performance over typical operating conditions for

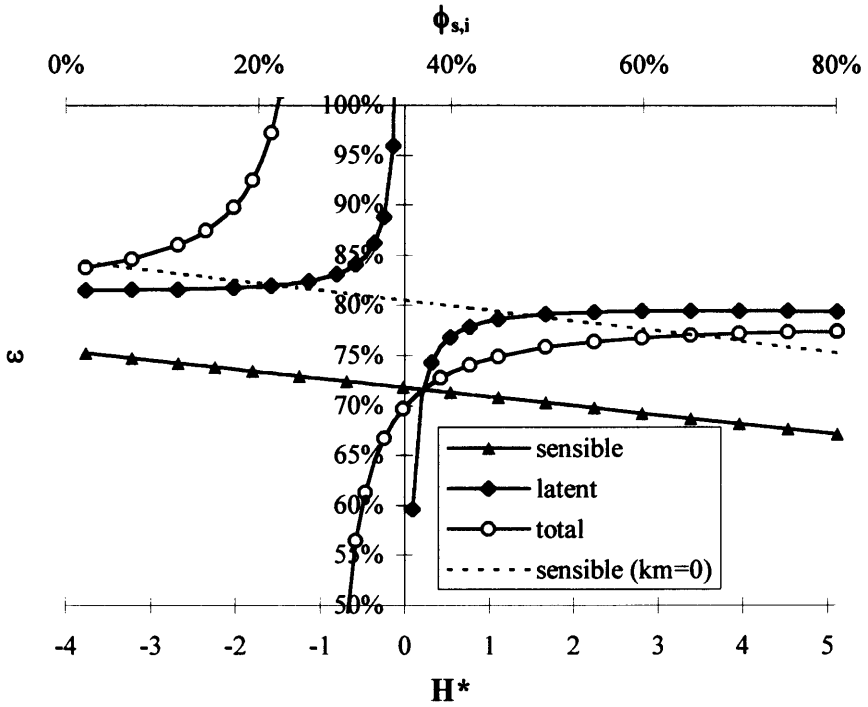

Fig. 13. Effectiveness versus H^* for the hot test conditions.

energy wheels. Type IM and IIIM sorption curves are also acceptable for energy wheels, but Type IE and Type IIIE sorption curves have poor performance at certain humidities.

The sensible, latent and total effectiveness correlations, developed in this paper, agree with over 600 simulated values within ± 2.5, ± 2 and $\pm 2.5\%$, respectively. The correlations allow the designer to calculate effectiveness from known parameters and are:

$$\varepsilon_s = \frac{NTU_o}{1+NTU_o}\left(1-\frac{1}{7.5Cr_o^*}\right) - \left[\frac{0.26\left(\dfrac{Cr_o^*}{Wm^2 Crm_o^*}\right)^{0.28}}{7.2(Cr_o^*)^{1.53}+\dfrac{210}{(NTU_o)^{2.9}}-5.2}+\frac{0.31\eta}{(NTU_o)^{0.68}}\right]H^* \tag{17}$$

$$\varepsilon_l = \frac{NTU_o}{1+NTU_o}\left(1-\frac{1}{0.54(Cr^*_{mt,o})^{0.86}}\right)\times\left(1-\frac{1}{(NTU_o)^{0.51}(Cr^*_{mt,o})^{0.54}H^*}\right) \quad \text{and} \tag{18}$$

$$\varepsilon_t = \frac{\varepsilon_s+\varepsilon_l H^*}{1+H^*} \tag{19}$$

where:

$$NTU_o = \frac{1}{(\dot m C_{p_a})_{min}}\left[\frac{1}{(hA_s)_s}+\frac{1}{(hA_s)_e}\right]^{-1} \tag{20}$$

$$Cr_o^* = \frac{(MC_p)_m N}{(\dot m C_{p_a})_{min}}, \tag{21}$$

$$Crm_o^* = \frac{M_{d,dry}N}{\dot m_{min}} \tag{22}$$

$$Cr^*_{mt,o} = (Crm_o^*)^{0.58}Wm^{0.33}\left(\frac{\partial u}{\partial\phi}\bigg|_{\phi_{ave}}\right)^{0.2}\times(Cr_o^*)^{1.13}\left(\frac{e^{\left(\frac{1482}{T_{ave}}\right)}}{47.9}-1.26(\phi_{ave})^{0.5}\right)^{4.66} \quad \text{and} \tag{23}$$

$$H^* = \frac{\Delta H_l}{\Delta H_s} = \left(\frac{\Delta H_s}{\Delta H_l}\right)^{-1} - 1 = 2500\frac{\Delta W}{\Delta T}. \tag{24}$$

The above correlations apply for the following range of parameters: $0 \leqslant \eta \leqslant 0.1$, $-6 \leqslant H^* \leqslant 6$, $2 \leqslant NTU_o \leqslant 10$, $3 \leqslant Cr_o^* \leqslant 10$, $1 \leqslant Cr_o^*/Crm_o^* \leqslant 5$, $0.1 \leqslant Wm \leqslant 0.5$, $C = 1$ and $C^* = 1$. These effectiveness correlations, although quite complex, are simpler to use than numerical models and will permit manufacturers and HVAC engineers to optimize energy wheel performance and life cycle cost savings for air conditioning applications in different climates for a range of building operating conditions.

References

[1] R.K. Shah, E.K. Subbarao, R.A. Mashelkar, Heat Transfer Equipment Design, Hemisphere, New York, 1988.

[2] W.M. Kays, A.L. London, Compact Heat Exchangers, McGraw-Hill, Toronto, 1984.

[3] F.P. Incropera, D.P. Dewitt, Fundamentals of Heat and Mass Transfer, 4th ed., Wiley, Toronto, 1996, ch. 11.

[4] C.J. Simonson, R.W. Besant, Heat and moisture transfer in desiccant coated rotary energy exchangers: Part I—numerical model, Int. J. HVAC & 3R Res. 3 (4) (1997) 325–350.

[5] C.J. Simonson, Heat and moisture transfer in energy wheels, Ph.D. thesis, University of Saskatchewan, Saskatoon, Saskatchewan, Canada, 1998.

[6] ASHRAE Standard 84-1991, Method of testing air-to-air heat exchangers, American Society of Heating, Refrigerating and Air Conditioning, Engineers Inc., Atlanta, 1991.

[7] CSA Standard C439-M1988, Standard methods of test for rating the performance of heat recovery ventilators, Canadian Standards Association, Rexdale, Ontario, Canada, 1988.

[8] ENV Standard 308-1996, Heat exchangers—test procedures for establishing performance of air-to-air and flue gases heat recovery devices, European Committee for Standardization, 1996.

[9] H.N. Gawley, D.R. Fisher, The effectiveness and rating of air-to-air heat exchangers, ASHRAE Trans. 81 (2) (1975) 401–409.

[10] H. Klein, S.A. Klein, J.W. Mitchell, Analysis of regenerative enthalpy exchangers, Int. J. Heat Mass Transfer 33 (1990) 735–744.

[11] G. Stiesch, S.A. Klein, J.W. Mitchell, Performance of rotary heat and mass exchangers, Int. J. HVAC & R Res. 1 (4) (1995) 308–323.

[12] W. Zheng, W.M. Worek, D. Novosel, Control and optimization of rotational speeds for rotary dehumidifiers, ASHRAE Trans. 99 (1) (1993) 825–833.

[13] C.J. Simonson, D.L. Ciepliski, R.W. Besant, Determining the performance of energy wheels: Part I—experimental and numerical methods, ASHRAE Trans. 105 (1) (1999).

[14] C.J. Simonson, D.L. Ciepliski, R.W. Besant, Determining the performance of energy wheels: Part II—experimental data and numerical validation, ASHRAE Trans. 105 (1) (1999).

[15] D.L. Ciepliski, R.W. Besant, C.J. Simonson, Some recommendations for improvements to ASHRAE standard 84-1991, ASHRAE Trans. 104 (1) (1998) 1651–1665.

[16] K. Rengarajan, D.B. Shirey III, R.A. Raustad, Cost-effective HVAC technologies to meet ASHRAE Standard 62-1989 in hot and humid climates, ASHRAE Trans. 102 (1) (1996) 166–182.

[17] D.B. Shirey III, K. Rengarajan, Impact of ASHRAE Standard 62-1898 on small Florida offices, ASHRAE Trans. 102 (1) (1996) 153–165.

[18] I.L. Maclaine-cross, A theory of combined heat and mass transfer in regenerators, Ph.D. thesis, Monash University, Australia, 1974.

[19] C.J. Simonson, R.W. Besant, G.W. Wilson, Condensation and frosting in energy wheels, in: K. Vafai, J.L.S. Chen (Eds.), Proceedings ASME 32nd National Heat Transfer Conference, HTD 339(1), Current Developments in Numerical Simulation of Heat and Mass Transfer, ASME, New York, 1997, pp. 161–169.

[20] T.J. Lambertson, Performance factors of a periodic-flow heat exchanger, Trans. ASME 80 (1) (1958) 586–592.

[21] R.K. Shah, Thermal design theory for regenerators, in: S. Kakaç, A.E. Bergles, F. Mayinger (Eds.), Heat Exchangers: Thermal-Hydraulic Fundamentals and Design, Hemisphere, New York, 1981, pp. 721–763.

[22] C.J. Simonson, R.W. Besant, Heat and moisture transfer in energy wheels during sorption, condensation and frosting conditions, ASME J. Heat Transfer 120 (3) (1998) 699–708.

[23] C.J. Simonson, R.W. Besant, Heat and moisture transfer in desiccant coated rotary energy exchangers: Part II—validation and sensitivity studies, Int. J. HVAC & R Res. 3 (4) (1997) 351–368.

[24] R.K. Shah, Counter flow rotary regenerator thermal design procedures, in: R.K. Shah, E.K. Subbarao, R.A. Mashelkar (Eds.), Heat Transfer Equipment Design, Hemisphere, New York, 1988, pp. 267–296.

[25] S.V. Patankar, Numerical Heat Transfer and Fluid Flow, Hemisphere, New York, 1980.

[26] C.J. Simonson, W. Shang, R.W. Besant, Part load performance of energy wheels, ASHRAE Trans. (1998) submitted for publication.

[27] R.K. Collier, T.S. Cale, Z. Lavan, Advanced desiccant materials assessment: Phase 1, Gas Research Institute, Report GRI-86-0182, Chicago, 1986.

[28] R.K. Shah, A.L. London, in: T.F. Irvine, Jr., J.P. Hartnett (Eds.), Advances in Heat Transfer: Laminar Flow Forced Convection in Ducts: A Source Book for Compact Heat Exchanger Analytical Data, Academic Press, New York, 1978.